Article

# Electrochromogenic Detection of Live Bacteria Using Soluble and Insoluble Prussian Blue

Amparo Ferrer-Vilanova,* Yasmine Alonso, Josune J Ezenarro, Sara Santiago, Xavier Muñoz-Berbel, and Gonzalo Guirado*

Cite This: *ACS Omega* 2021, 6, 30989−30997

Read Online

ACCESS | Metrics & More | Article Recommendations | Supporting Information

**ABSTRACT:** Microbial detection is crucial for the control and prevention of infectious diseases, being one of the leading causes of mortality worldwide. Among the techniques developed for bacterial detection, those based on metabolic indicators are progressively gaining interest due to their simplicity, adaptability, and, most importantly, their capacity to differentiate between live and dead bacteria. Prussian blue (PB) may act as a metabolic indicator, being reduced by bacterial metabolism, producing a visible color change from blue to colorless. This molecule can be present in two main forms, namely, the soluble and the insoluble, having different properties and structures. In the current work, the bacterial-sensing capacity of soluble and insoluble PB will be tested and compared both in suspensions as PB-NPs and after deposition on transparent indium tin oxide-poly(ethylene terephthalate) (ITO-PET) electrodes. In the presence of live bacteria, PB-NPs are metabolized and completely reduced to the Prussian white state in less than 10 h for soluble and insoluble forms. However, when electrodeposited on ITO-PET substrates, less than 1 h of incubation with bacteria is required for both forms, although the soluble one presents faster metabolic reduction kinetics. This study paves the way to the use of Prussian blue as a metabolic indicator for the early detection of bacterial infection in fields like microbial diagnostics, surface sterilization, food and beverage contamination, and environmental pollution, among others.
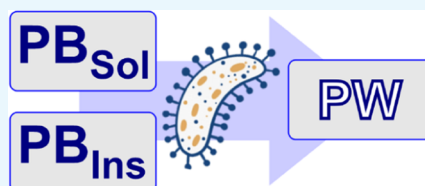
## INTRODUCTION

Microbial detection is crucial for the control and prevention of infectious diseases, being one of the leading causes of mortality worldwide.[1] Standard microbial detection methods based on cell culturing and colony counting[2] are now being replaced by simpler and less tedious technologies. Among them, the polymerase chain reaction (PCR),[3] based on the identification of specific oligonucleotide sequences (e.g., genes), and the enzyme-linked immunosorbent assay (ELISA),[4] consisting of the recognition of specific external proteins (e.g., receptors) with selective antibodies, are now the most commonly used in the laboratories. To attain the challenge of microbial detection out of the laboratory, portable and miniaturized versions of these techniques have been developed,[5] also in the form of biosensors selective to DNA strains (DNA sensors)[6] or to antigens/antibodies (immune sensors).[7] The main limitation of these systems is the differentiation between live and dead bacteria. This is particularly relevant in the case of DNA-based technologies for the high stability of oligonucleotide strains, although some strategies to distinguish live/dead bacteria have been already developed.[8] There are commercial kits such as live/dead Backlight bacterial viability kit and live/dead cell viability assay kit, which are gaining popularity. However, these kits are very expensive and the toxicity of their dyes makes them difficult to apply in continuous viability measurements. Alternatives involving the detection of metabolically produced adenosine triphosphate (ATP),[9] defined substrate technology,

e.g., COLIPAT,[10] the use of fluorescent nanomaterials,[11,12] or the use of metabolic indicators[13,14] such as ferricyanide[15] or Presto Blue[16] are now becoming more popular for their simplicity and rapid in situ response. Among them, metabolic indicators are preferred for being more general than those based on defined substrate technologies, restricted to some bacterial types/families, and simpler than ATP detection or the use of fluorescent dyes, which requires instrumentation to detect bioluminescence or fluorescence, respectively; with metabolic indicators, the color change can be even detected with the bare eye.[17]

Metabolic indicators are molecules with capacity to "accept electrons" from proteins involved in the electron transport chain (ETC), e.g., c-type cytochromes, and/or redox-active shuttle molecules secreted by bacteria.[18,19] Ferricyanide is among the most common metabolic indicator, reporting on both Gram-positive and Gram-negative bacteria.[20−23] Metabolic reduction of ferricyanide to ferrocyanide involved the color change of the molecule from pale yellow to colorless, which is hard to see with the naked eye. Commercial

alternatives such as alamar Blue present more intense color changes but are still difficult to detect visually and a fluorescence measurement is recommended by the supplier.

Ferric hexacyanoferrate, also known as Prussian blue (PB), is a derivate of the previous molecules with an intense blue color (i.e., extinction molar coefficient almost 50 times higher than ferricyanide) and becoming uncolored after reduction to Prussian white (PW).[24−26] Due to its intense color change and biocompatibility, PB has been already employed as a redox mediator in the development of sensors and biosensors.[27−29] Furthermore, there are preliminary results supporting its ability to interact with the ETC of iron-reducing organisms,[30] and in our previous work, we demonstrated that it can detect both, Gram-positive and Gram-negative bacteria,[31] although its capacity as a bacterial electron acceptor and the differences between its soluble and insoluble forms have been poorly studied. PB-NPs have a tridimensional network structure with a remaining charge that is compensated by either potassium or ferric ions. When the charge is compensated by potassium ions, PB is known as "soluble" ($PB_{Sol}$) since the small size of the NPs allows their suspension in solution with low deposition kinetics. In contrast, ferric counterions lead to what is called "insoluble" PB ($PB_{Ins}$), containing aggregations of NPs that tend to precipitate quickly.[32,33] Schemes for the two structures are shown in Figure 1. Both forms of PB present similar, but
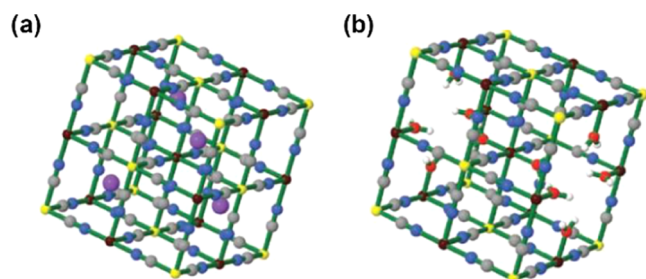


**Figure 1.** Structures of the PB forms. (a) Structure of $PB_{Sol}$, with the centers of the cubic cells occupied by $K^+$ ions. (b) Structure of $PB_{Ins}$, where the coordinative sphere of $Fe^{III}$ is completed by water. Colors of the atoms: $Fe^{II}$ (yellow), $Fe^{III}$ (brown), C (gray), N (blue), K (violet), O (red), and H (white). The figure is obtained from ref 34.

not identical, color changes and standard redox potentials. In this article, the electrochromic differences of the two PB forms in bacterial detection are extensively studied and discussed both in a suspension and when immobilized in electrodes for optical and/or electrochemical transduction.

## ■ RESULTS AND DISCUSSION

**Study of the Electrochromic Properties of Soluble and Insoluble PB-NPs.** For a better understanding of the bacterial-sensing mechanism, optical and electrochemical properties of both $PB_{Sol}$ and $PB_{Ins}$ were studied. Although both forms of PB were insoluble in most solvents, $PB_{Sol}$ was partially peptized and solubilized in oxalic acid.[35] To avoid the physical adsorption of colloidal PB on the electrode surface, a platinum mesh was used as working electrode (WE). In these experimental conditions, 1 mM $PB_{Sol}$ was measured by cyclic voltammetry (CV) at 20 mV s$^{-1}$ in 0.1 M KCl supplemented with 0.1 M oxalic acid, obtaining repeatable and reliable electrochemical recordings (Figure 2a).

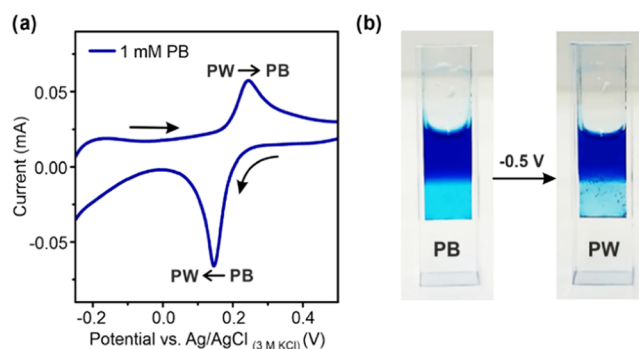In the ETC of *Escherichia coli*, the exchange of electrons is produced between several primary dehydrogenases and



**Figure 2.** Electrochemical and optical characterization of $PB_{Sol}$ in suspension. (a) CV of an aqueous suspension of 1 mM $PB_{Sol}$ in a 0.1 M KCl and 0.1 M oxalic acid medium at 20 mV s$^{-1}$. (b) Suspension color change obtained after applying −0.5 V for 2 min in the same previous conditions.

terminal reductases, which are linked by three quinones: ubiquinone ($E° = 0.1$ V vs NHE), dimethyl menaquinone (MQ) ($E° = 0.04$ V vs NHE), and MQ ($E° = −0.08$ V vs NHE).[36] From Figure 2a, a standard redox potential of 0.2 V vs Ag/AgCl (3M KCl) (0.4 V vs NHE) was obtained, which was theoretically appropriated to oxidize the proteins and mediators involved in the ETC. Even cytochrome *d*, the most positive component of *E. coli* ECT with a midpoint potential of 0.27 V vs NHE,[37] may be oxidized by PB-NPs.

To simulate the metabolic reduction of colloidal PB-NPs by bacterial metabolism, a potential of −0.5 V (vs Ag/AgCl (3 M KCl)) was applied to the NP suspension for 2 min. As shown in Figure 2b, a lighter color of the solution was obtained, associated with the PB reduction, where the typical colloidal nature of the $PB_{Sol}$ suspension could also be appreciated with the bare eye.

On the other hand, $PB_{Ins}$ could not be peptized/solubilized with oxalic acid and presented fast sedimentation kinetics that impeded its characterization directly in solution. For this reason, $PB_{Ins}$ was electrodeposited on conductive and transparent indium tin oxide-poly(ethylene terephthalate) (ITO-PET) electrodes for electrochemical and optical analysis. Two $PB_{Ins}$ electrodeposition procedures were performed and compared, namely, potentiostatic (constant potential) and galvanostatic (constant charge). Electrodeposition results are presented in Figure 3, including (i) images of the electrodeposited electrodes at different electrodeposition times, (ii) scanning electron microscopy (SEM) images of electrodes electrodeposited for 80 s, and (iii) CVs obtained from all electrodeposited electrodes. The thickness of the electrodeposited layers was determined by atomic force microscopy (AFM) and is presented in Figure 4.

With both electrodeposition strategies, longer electrodeposition times produced thicker PB films with deeper color intensities and larger current magnitudes in the CVs. Conversely, peak separation also increased with the electrodeposition time by a reduction of charge transfer capacity when increasing the thickness of the electrodeposited layer. In both cases, an $E°$ of 0.12 V vs Ag/AgCl (3M KCl) (0.32 vs NHE) was obtained, slightly smaller than that obtained by the soluble form in suspension but sufficiently high to react with most of the redox components of the bacterial ETC. Comparing both techniques, potentiostatic electrodeposition provided higher peak and color intensities, which are associated with the formation of larger particles and a thicker
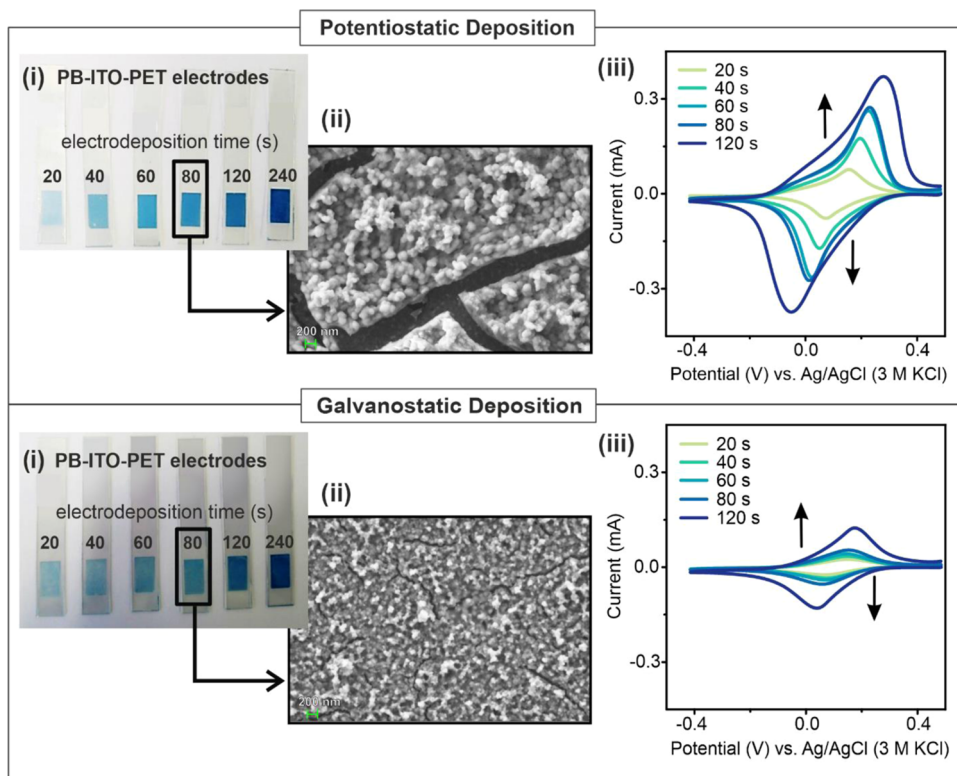
**Figure 3.** Comparative scheme for $PB_{Ins}$ electrodeposition on ITO-PET electrodes by potentiostatic and galvanostatic techniques. Different parameters are shown, such as (i) images of the PB-electrodeposited electrodes at different deposition times, (ii) SEM images of PB electrodeposited for 80 s, and (iii) CVs recorded from PB-deposited electrodes.
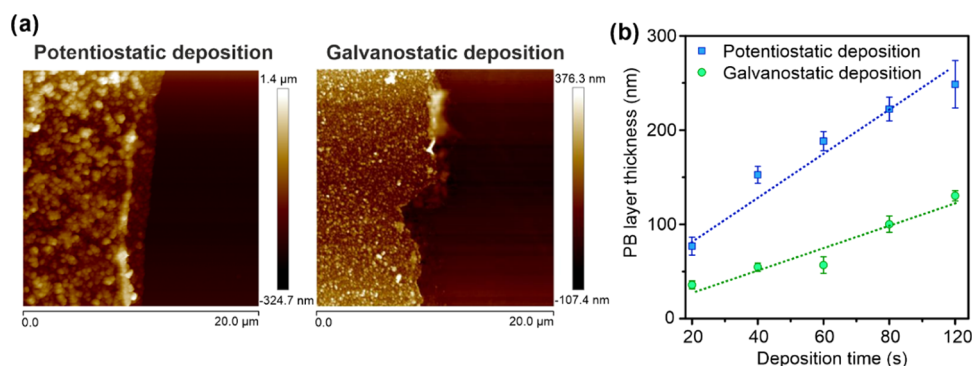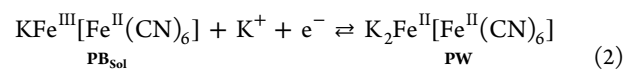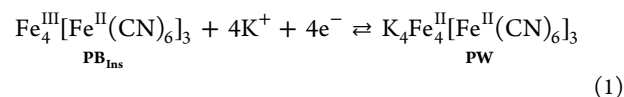


**Figure 4.** PB-layer thickness for potentiostatic and galvanostatic eletrodeposition techniques. (a) AFM images for PB electrodeposited on ITO-PET electrodes potentiostatically and galvanostatically for 80 s. (b) PB-layer thickness measured on all of the modified electrodes by the AFM technique versus the deposition time ($n = 5$).

PB layer, as observed by SEM (Figure 3) and AFM (Figure 4a; all images in Figures S1 and S2). Further, 80 s of potentiostatic electrodeposition, which corresponded to a PB layer of around 200 nm (Figure 4b), was chosen as the optimal condition for spectroelectrochemical studies.

In spectroelectrochemical assays, the electrodeposited electrodes were submerged in the cell containing 1 M KCl, and 10 CVs were registered between 0.7 and −0.4 V (vs Ag/AgCl (3M KCl)) at 20 mV s$^{-1}$. Along the cycles, small differences were observed between the first scan and the other nine. Regarding the standard redox potential value, it was a clear shift of approximately 20 mV (Figure 5a). The spectroscopic change was more evident, where the PB band initially at 720 nm was shifted to 710 nm, showing a decrease in the absorbance peak value after the development of 10

cycles (Figure 5b).[38] The shift in the peak potential and absorbance magnitude suggested structural changes in PB along with the reduction to PW and reoxidation. Although still controversial, the following mechanism was proposed based on previous studies,[39−42] which is illustrated in eqs (1) and (2)

$$\underset{\textbf{PB}_{\textbf{Ins}}}{Fe_4^{III}[Fe^{II}(CN)_6]_3} + 4K^+ + 4e^- \rightleftarrows \underset{\textbf{PW}}{K_4Fe_4^{II}[Fe^{II}(CN)_6]_3}$$

(1)

$$\underset{\textbf{PB}_{\textbf{Sol}}}{KFe^{III}[Fe^{II}(CN)_6]} + K^+ + e^- \rightleftarrows \underset{\textbf{PW}}{K_2Fe^{II}[Fe^{II}(CN)_6]}$$

(2)

$PB_{Ins}$ was first electrodeposited on the ITO-PET electrodes. When potential cycles were applied in K$^+$-containing media, potassium cations occupied the PB cavities during PW
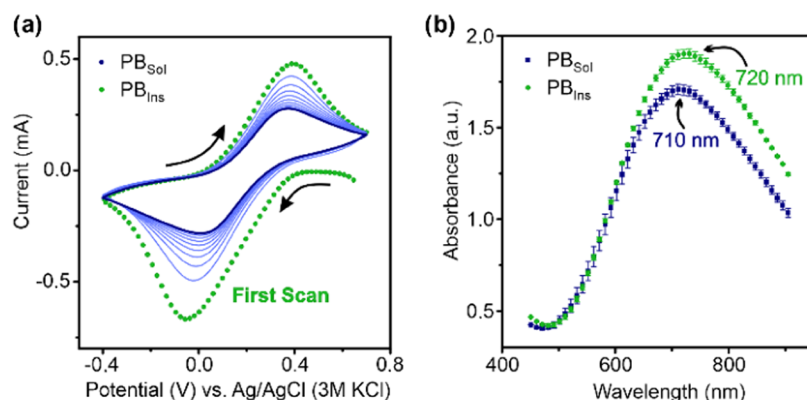
**Figure 5.** Spectroelectrochemical differences between $PB_{Sol}$ and $PB_{Ins}$. (a) Development of 10 CVs from 0.7 to −0.4 V vs Ag/AgCl (3M KCl) at 20 mV s$^{-1}$ to the electrodeposited PB films. The first scan corresponds to $PB_{Ins}$ (green), while the rest correspond to the progressive formation of $PB_{Sol}$ (dark blue). (b) Absorbance spectrum obtained from freshly electrodeposited PB ($PB_{Ins}$, in green) and after applying 10 CVs ($PB_{Sol}$, in blue).
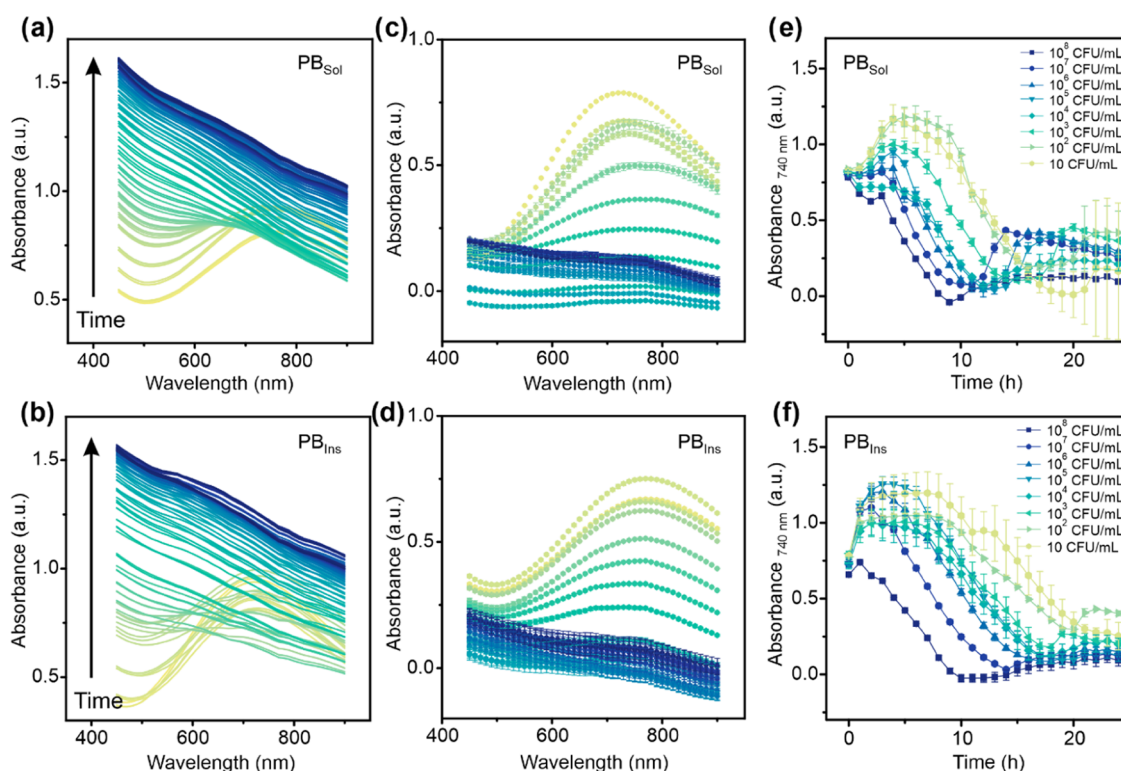


**Figure 6.** Bacterial-sensing activity of PB-NPs in suspension. Absorbance spectra obtained over time for (a) $PB_{Sol}$ and (b) $PB_{Ins}$, when incubated with a bacterial concentration of 10$^8$ CFU mL$^{-1}$ in an MH medium (pH 6.2). Absorbance spectra resulting when data from bacterial scattering were extracted for (c) $PB_{Sol}$ and (d) $PB_{Ins}$. Absorbance values at 740 nm obtained from the previous graphs versus reaction time after *E. coli* inoculation at different concentrations (between 10 and 10$^8$ CFU mL$^{-1}$) with (e) $PB_{Sol}$ and (f) $PB_{Ins}$, during 24 h in an MH medium (pH 6.2). For all graphs shown, $n$ = 3.

oxidation, transforming the initial $PB_{Ins}$ into $PB_{Sol}$. Furthermore, the decrease in the value of the peak current among cycles, as shown in Figure 5a, confirmed the loss of iron atoms in the PB structure when $PB_{Ins}$ was converted into $PB_{Sol}$. Although indistinguishable by the bare eye, both soluble and insoluble forms of electrodeposited PB presented slightly different optical and electrochemical properties (a difference of about 20 mV in the standard redox potential, 10 nm in the absorbance peak, and a decrease in current and absorbance values), which may affect their bacterial-sensing capacity.

**Bacterial-Sensing Activity of Soluble and Insoluble PB-NPs in Suspension.** Bacterial-sensing activity of both soluble and insoluble forms of PB was analyzed and compared

using *E. coli* as a model microorganism. PB suspensions were prepared with the same initial absorbance magnitude of 0.9 AU, corresponding to theoretical concentrations of 0.28 mM $PB_{Sol}$ and 0.07 mM $PB_{Ins}$. The molar extinction coefficient of both was estimated using a spectrochemical cell with different light paths, as shown in Figure S3a and S3b, Absorbance values were obtained at 716 nm and the linear regression was calculated for $PB_{Sol}$ and $PB_{Ins}$ (Figure S3b). Molar extinction coefficient values of 8.4 × 10$^3$ and 3.4 × 10$^4$ M$^{-1}$ cm$^{-1}$ were obtained for soluble and insoluble PB, respectively. These values were close to 3.0 × 10$^4$ M$^{-1}$ cm$^{-1}$, the theoretical molar extinction coefficient reported for $PB_{Sol}$ at 700 nm.[43]
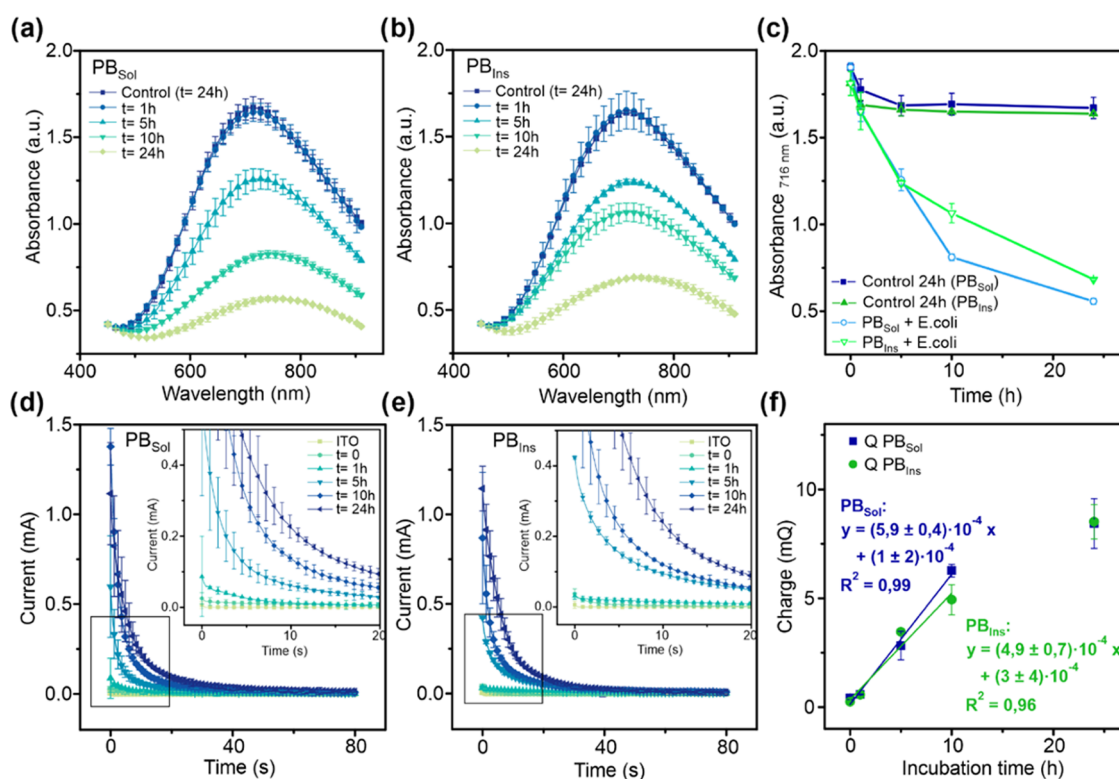
**Figure 7.** Bacterial-sensing activity of PB-NPs electrodeposited on ITO-PET electrodes. Absorbance spectra of the PB-electrodeposited electrodes, obtained after incubation with a bacterial concentration of $10^8$ CFU mL$^{-1}$ at different times (1, 5, 10, and 24 h) for (a) PB$_{Sol}$ and (b) PB$_{Ins}$. As control, PB electrodes were submerged in an MH medium (pH 6.2) ($n = 3$). (c) Absorbance values at 716 nm (obtained from the previous graphs) over incubation time for PB$_{Sol}$ and PB$_{Ins}$ electrodeposited electrodes and their respective controls ($n = 3$). The chronoamperometry curve of the PB-electrodeposited electrodes, obtained by applying 0.6 V for 80 s after incubation with a bacterial concentration of $10^8$ CFU mL$^{-1}$ at different times (1, 5, 10, and 24 h) for (d) PB$_{Sol}$ and (e) PB$_{Ins}$ ($n = 3$). (f) Relationship between the charge obtained by integrating the curve at the chronoamperometry versus the incubation time for PB$_{Sol}$ (blue squares) and PB$_{Ins}$ (green circles).

PB-NP suspensions were incubated with *E. coli* concentrations between 10 and $10^8$ CFU mL$^{-1}$ for 24 h, and the absorbance spectrum was recorded for each hour with a plate reader. Results for soluble and insoluble PB, when incubated with a bacterial concentration of $10^8$ CFU mL$^{-1}$, are illustrated in Figure 6a,6b, respectively. In both cases, initially, the PB peak around 700 nm is observed, which disappeared over time due to its reduction to PW by bacterial metabolism. However, a general increment of absorbance in the full spectrum is observed due to the scattering produced by the bacteria growth, which was higher at the lowest wavelengths. To better observe the color shift produced by metabolic reduction of PB-NPs, the contribution of bacterial scattering was subtracted. After scattering subtraction, the peak decrease at 700 nm corresponding to the reduction from PB to PW was clearly observed for PB$_{Sol}$ and PB$_{Ins}$, as shown in Figure 6c,d, respectively. Even considering only the color change of the PB-NPs, scattering was still observed at low wavelengths, probably resulting from the insolubility of PB-NPs. It is clearly observed that this light scattering associated with the presence of PB-NPs was more intense in the case of PB$_{Ins}$, which, in fact, produced larger particles more susceptible to scatter light. Although the rates of the color change were larger for higher bacterial concentrations, metabolic reduction activity was observed in all bacterial samples evaluated. The peak reduction kinetics at 740 nm for 24 h of incubation is represented in Figure 6e,6f for soluble and insoluble PB, respectively. In the case of $10^8$ CFU mL$^{-1}$, a complete reduction to PW was

achieved in less than 10 h in both cases. For the lowest concentration (10 CFU mL$^{-1}$), the total color change was accomplished after 20 h of incubation. Observing the resulting graphs, at the beginning of the experiment, there is a tendency to increase the absorbance values, which end up decreasing over time. This increment was higher at the lowest bacterial concentrations and may be related to the scattering produced by PB-NPs since more time was needed to be metabolized by bacteria. Comparing both forms, although the differences are small, the reduction to the PW state in general terms was achieved faster in the case of PB$_{Sol}$. This fact was associated with its higher solubility, which facilitated the PB-NP diffusion in the medium to accept electrons from bacterial ETC. Although still controversial, these differences may be associated with the different compositions of both PB forms and their reactivity with bacteria and other components of the medium, e.g., potassium ions.

**Bacterial-Sensing Activity of PB-NPs Electrodeposited on ITO-PET Electrodes.** After the potentiostatic electrodeposition of soluble and insoluble PB on ITO-PET electrodes, their bacterial-sensing activity was also studied and compared. Electrodes freshly electrodeposited were used as PB$_{Ins}$, while those cycled in a KCl 1 M medium were used to test the PB$_{Sol}$ behavior. Both types of PB films were incubated with an *E. coli* suspension of $10^8$ CFU mL$^{-1}$ and their metabolic reduction activity was analyzed by optical and electrochemical measurements at different times: 0, 1, 5, 10, and 24 h. Spectra obtained at these times are shown in Figure

7a,b for soluble and insoluble PBs, respectively. As a control, electrodes were submerged in an MH medium (pH 6.2) and the absorbance was measured after 24 h. The reduction in the PB absorbance peak by bacterial metabolism was clearly observed after 1 h of incubation. To compare the reduction rates for both forms of PB, Figure 7c shows the absorbance value at 716 nm for the control and the samples in contact with bacteria. $PB_{Sol}$ showed faster kinetics of reduction to PW when in contact with bacteria, while both controls remained constant along the experiment.

Similarly, at the described incubation times, electrochemical measurements were carried out using chronoamperometry by applying a constant potential of 0.6 V vs Ag/AgCl (3M KCl) for 80 s. As a control, ITO-PET electrodes without any treatment were used. The resulting graphs for soluble and insoluble PBs are illustrated in Figure 7d,7e, respectively. As shown, longer incubation times resulted in higher metabolic reduction of PB to PW. Thus, when a positive potential was applied, the area of the curve in the obtained chronoamperometry was proportional to the PB reduced by bacteria or the PW reoxidized. In the graphs, it is clearly shown how at the beginning of the experiment, there was no PB reduced, while after 24 h of incubation, $PB_{Sol}$ and $PB_{Ins}$ showed larger areas under the curve. To study the kinetics of the process, the charge obtained after the chronoamperometry was calculated by integrating those areas. The relationship between the charge obtained and the incubation times is plotted in Figure 7f for $PB_{Sol}$ and $PB_{Ins}$. Logically, the longer the incubation time, the more the amount of PB was reduced by bacteria, which produced more charge when reoxidized. In both cases, the metabolic reduction of PB by bacteria could be observed after 1 h of incubation. However, the slope for $PB_{Sol}$ was 18% higher than for $PB_{Ins}$, which entails faster kinetics for the $PB_{Sol}$-sensing capacity. In addition, the limit of detection was calculated based on the standard deviation of the blank and the slope for both processes ($3 \sigma_{(t=0)}$/slope), being 4 min for the soluble and 8 min for the insoluble one. Analogously, the limit of quantification ($10 \sigma_{(t=0)}$/slope) was calculated from the regression data of Figure 7, and results showed that 28 min would be needed to detect the constant bacterial concentration used ($10^8$ CFU mL$^{-1}$) for the $PB_{Ins}$, while for the $PB_{Sol}$, changes could be observed in only 14 min.

These differences may be related to the different structures presented for both forms. As shown in eqs 1 and 2, they differ in formula (molecular mass and the number of iron atoms in the structure) and in the number of electrons exchanged. According to Faraday's Law, the charge of the curve can be related to the number of moles of PB reduced by bacterial metabolism (eq 3)

$$n = \frac{Q}{zF} \tag{3}$$

where $n$ is the number of moles of PB, $Q$ is the calculated charge of the curve (C), $z$ is the number of electrons involved in the electrochemical process, and F is the Faraday constant (96485 C mol$^{-1}$). This equation was applied for $PB_{Sol}$ and $PB_{Ins}$ metabolic reduction processes. Considering the same value of charge for both and simplifying the equation, the following relationship between the number of moles of soluble and insoluble PB is obtained in (eq 4)

$$\frac{n_S}{n_I} = 4 \tag{4}$$

Although the amount of charge obtained in the reduction of PB by bacterial metabolism is similar for $PB_{Sol}$ and $PB_{Ins}$, there is a difference between the number of moles reduced. Figure 8
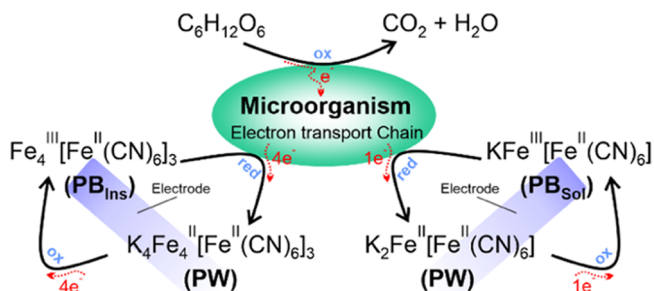


**Figure 8.** Scheme of the electron pathway during the electrochemical detection process.

illustrates the electron pathway through the electrochemical detection process. Bacteria oxidize the organic material (generally glucose is used as a carbon source) to obtain energy. Electrons derived from this process are passed through the bacterial electron transport chain in the plasma membrane to finally reduce the electrodeposited PB to the colorless PW state. PW on the electrode is reoxidized to the initial PB and the current produced is proportional to the amount of PB metabolized by bacteria during the incubation period. Therefore, for each mole of $PB_{Sol}$ metabolized by bacteria, four moles of $PB_{Ins}$ are needed to produce the same amount of charge. This fact is closely linked to the number of iron atoms presented in each structure. The $PB_{Ins}$ structure presents four iron (III) atoms, thus four electrons are needed to switch the PW form, while $PB_{Sol}$ only needs one electron to achieve the reduction process. Therefore, the metabolic reduction kinetics from PB to PW is four times higher for the soluble form than for the insoluble one.

Compared to other live/dead detection methods, detection times may appear longer. However, as demonstrated in our previous work,[31] this study is developed for the future application in smart products, in which the detection will be produced in situ and without the need for sample collection, transport, and/or treatment/processing. Other works present shorter detection times;[44,45] however, the time dedicated to samples' collection, transport, and preparation (24−48 h) is even longer than the one presented here. Although less than 1 h is a reasonable time when considering a practical application, e.g., detection of microbial pollution, bacterial concentrations necessary to produce this change are still high. To reach the small detection limits of current regulations, the use of more sensitive transduction mechanisms, e.g., amperometric detection by incorporating electrodes on different substrates, and/or preconcentration processes are currently being explored.

## ■ CONCLUSIONS

PB, due to its optical (high molar extinction coefficient) and electrochemical (suitable redox potential) properties, is an excellent candidate for bacterial detection either in solution or after deposition in solid-state transparent ITO-PET electrodes. The two main forms of PB, namely, soluble and insoluble, present differences in terms of the structure (the counter ion in the insoluble form is an iron atom and in the soluble form is potassium), absorption capacity (a difference in the absorption peak of 10 nm is shown, and the molar absorption coefficient

for the insoluble is four times higher than for the soluble one), and redox activity (both present a difference of approximately 20 mV, having the soluble form a smaller redox potential, more suitable to react with the proteins in the ETC). Both forms are metabolized by bacteria, changing their redox state and producing an intense color change detectable even by the bare eye. However, the soluble form presents some advantages in electrochemical detection, i.e., faster metabolic reduction kinetics observed at a higher slope value obtained from the quantification of the charge produced by the process. This difference may be attributed to more suitable redox potential and the presence of a single iron ion in the structure of the soluble form, while the insoluble form requires the reduction of four iron atoms for producing the color change. Therefore, this study elucidates the potential of PB-NPs to be used as metabolic indicators for the detection of the presence of living bacteria in different environments, e.g., liquids, solids, or air, with potential application in many sectors such as clinical diagnostics, food and beverage contamination, or water pollution, among others.

## ■ EXPERIMENTAL SECTION

**Reagents.** Potassium ferricyanide ($K_3[Fe(CN)_6]$), iron(II) chloride ($FeCl_2$), hydrogen chloride (HCl 37%), and Mueller−Hinton broth 2 (MH) were purchased from Sigma-Aldrich (Spain). Iron (III) chloride anhydrous ($FeCl_3$) was obtained from Fischer Scientific. Glucose was obtained from Panreac (Spain). Potassium chloride (KCl) and oxalic acid were purchased from Probus. All chemicals were used as received. Aqueous solutions were prepared using deionized water.

**Synthesis of PB-NPs.** PB-NPs were synthesized by a chemical reaction of ferric and hexacyanoferrate ions in an aqueous solution (i.e., water) until a dark blue colloid was formed.[33,46] For $PB_{Sol}$ synthesis, equimolar solutions (30 mM) of $FeCl_2$ and $K_3[Fe(CN)_6]$ were used. Concretely, 25 mL of the ferricyanide solution was slowly added to 25 mL of iron dichloride, resulting in a dark blue solution corresponding to $PB_{Sol}$ formation. On the other hand, $PB_{Ins}$ was synthesized by mixing 50 mL of 15 mM $K_3[Fe(CN)_6]$ with an excess of $FeCl_2$ (30 mL of a 0.1 M solution). In this case, the iron dichloride solution was the one added to the ferricyanide, leading to the formation of the dark blue precipitate corresponding to $PB_{Ins}$. The precipitate was left to deposit and cleaned twice with distilled water. In both cases, PB-NPs were stored refrigerated and protected from light until used.

**Electrochemical Measurements.** Electrochemical measurements were performed to evaluate the redox properties of suspensions of $PB_{Sol}$-NPs, i.e., the redox potential peak position and intensity, reversibility, and stability. A three-electrode electrochemical cell was used, containing a platinum mesh working electrode (WE) to avoid the physical adsorption of colloidal PB on the electrode surface, a platinum wire counter electrode (CE), and a Ag/AgCl (3M KCl) reference electrode (RE).

Electrochemical studies required the electrodeposition of PB-NPs on the WE surface. In this case, poly(ethylene terephthalate) sheets coated with conductive indium tin oxide (ITO-PET) substrates were used as WE. Two different PB electrodeposition procedures were used and compared, namely, potentiostatic and galvanostatic electrodeposition. Potentiostatic electrodeposition was based on previous publications.[47,48] Briefly, a solution containing equimolar concentrations of $K_3[Fe(CN)_6]$ and $FeCl_3$ (10 mM) in 1 M

HCl was prepared and immediately electrodeposited at a constant potential of 0.4 V vs Ag/AgCl (3M KCl). Electrodeposition times between 20 and 120 s were evaluated. In the galvanostatic electrodeposition, the previous solution was electrodeposited but this time at a constant charge of 40 $\mu$A cm$^{-2}$ (24 $\mu$A, when considering the active area of the WE, i.e., 0.6 cm$^2$). For comparison with potentiostatic electrodeposition, this charge was applied between 20 and 120 s. Both potentionstatically and galvanostatically modified ITO-PET electrodes were rinsed with deionized water to remove nonelectrodeposited molecules and air-dried before electrochemical studies.

Once electrodeposited and with the optimal conditions already selected, the films were cycled in K$^+$-containing media to obtain the $PB_{Sol}$ form. For this purpose, PB-ITO-PET electrodes were submerged in a cell containing 25 mL of 1 M KCl (pH ≈ 2.5), and 10 CVs were registered between 0.7 and −0.4 V (vs Ag/AgCl (3M KCl)) at 20 mV s$^{-1}$.[48]

Measurements were conducted using an electrochemical workstation $\mu$-Autolab Type III and controlled with software Nova 2.1.4 (Metrohm Autolab B.V.).

**Spectrochemical Measurements.** The electrochromic behavior of PB was studied using spectrochemistry in solution and a solid state after electrodeposition on ITO-PET substrates. Samples were analyzed using a spectrochemical setup including a halogen lamp (HL-2000-FHSA, Ocean Optics) as a light source, a spectrophotometer (QE65000, Ocean Optics), and a holder of the same branch for introducing the cuvette with the sample, which ensures a fixed position for the optical fibers and avoids the incidence of light during the measurement. As a cuvette, a thin layer of quartz glass with two different optical paths from BAS Inc. was used. A 1 cm optical path was employed to analyze $PB_{Sol}$ samples in suspension. For PB-electrodeposited ITO-PET electrodes, samples were analyzed directly after introduction into the quartz cuvette cell and the optical path was 1 mm. Optical measurements were acquired using a spectrophotometer and controlled by OceanView software.

**SEM and AFM Measurements.** The surface topology of a PB-electrodeposited layer was studied by scanning electron microscopy (SEM) using an AURIGA series en04 SEM (CarlZeiss). The layer thickness was analyzed by atomic force microscopy (AFM) using a Nanoscope IV Dimension 3100 (Veeco Instruments).

**Bacterial Culture Preparation.** *Escherichia coli* ATCC 25922 (*E. coli*) was incubated aerobically in a Luria-Bertani (LB) broth overnight (18 h) at 37 °C with shaking. After centrifugation (Eppendorf centrifuge AG R134A) at 2700*g* for 10 min, the pellet was collected and resuspended in an MH medium (pH adjusted to 6.2 with 1 M HCl) adjusting the bacterial concentration through optical density measurements in a spectrophotometer (Smartspec Plus spectrophotometer, Bio-rad, California). An optical density of 0.16−0.17 AU was considered equivalent to 10$^8$ colony-forming units per mL (CFU mL$^{-1}$). Suitable aliquots were cultured in agar plates and counted after incubation for adjustment of bacterial concentration.

**Evaluation of Bacterial-Sensing Activity of PB-NPs.** Optical measurements were used to evaluate the bacterial-sensing capacity of PB-NPs in suspension, either soluble or insoluble, as well as to evaluate the influence of the PB concentration in bacterial proliferation. Absorbance measurements were performed in 96-well plates using a Thermo

Electron Multiskan EX plate reader (VWR International, Pennsylvania) and Ascent software (VWR International, Pennsylvania) for data recording. PB and bacterial solutions were freshly prepared every day. Their concentrations were adjusted to the assay and mixed in an MH medium just before starting the experiment. The pH value of the medium was adjusted to 6.2 since PB is only stable in acidic pH media, according to the study realized in our previous work.[31] Absorbance spectra in the wavelength range between 400 and 900 nm were acquired every hour for the duration of the experiment, obtaining three replicates for each condition. In PB data analysis, the contribution of bacterial scattering was subtracted from absorbance spectra to simplify result interpretation. Spectrum lines were additionally smoothed using the Savitzky−Golay algorithm to remove background noise.

Bacterial-sensing capacity of the electrodeposited electrodes was evaluated optically and electrochemically. Electrodes were incubated with a bacterial concentration of $10^8$ CFU mL$^{-1}$ and measured at different times: 0, 1, 5, 10, and 24 h. Optical measurements were carried out as explained in the Spectrochemical measurement section. Electrochemical measurements were performed chronoamperometrically by applying a constant potential of 0.6 V vs Ag/AgCl (3M KCl) for 80 s. Both types of measures were performed in an MH medium (pH 6.2).

## ASSOCIATED CONTENT

### Ⓢ Supporting Information

The Supporting Information is available free of charge at https://pubs.acs.org/doi/10.1021/acsomega.1c03434.

AFM images of PB electrodeposited on ITO-PET electrodes by the potentiostatic technique (Figure S1), AFM images of PB electrodeposited on ITO-PET electrodes by the galvanostatic technique (Figure S2), scheme of the spectrochemical cell used to determine the molar extinction coefficient of PB$_{Sol}$ and PB$_{Ins}$ (Figure S3a), and absorbance measurements obtained at 716 nm for PB$_{Sol}$ and PB$_{Ins}$ by varying the light path and linear regression values (Figure S3b) (PDF)

## AUTHOR INFORMATION

### Corresponding Authors

**Amparo Ferrer-Vilanova** − *Institut de Microelectrònica de Barcelona (IMB-CNM, CSIC), Universitat Autònoma de Barcelona, 08193 Cerdanyola del Vallès (Barcelona), Spain;* ⓞ orcid.org/0000-0002-4223-8442; Email: amparo.ferrer@imb-cnm.csic.es

**Gonzalo Guirado** − *Departament de Química, Universitat Autònoma de Barcelona, 08193 Cerdanyola del Vallès (Barcelona), Spain;* Email: gonzalo.guirado@uab.cat

### Authors

**Yasmine Alonso** − *Departament de Química, Universitat Autònoma de Barcelona, 08193 Cerdanyola del Vallès (Barcelona), Spain*

**Josune J Ezenarro** − *Institut de Microelectrònica de Barcelona (IMB-CNM, CSIC), Universitat Autònoma de Barcelona, 08193 Cerdanyola del Vallès (Barcelona), Spain;* ⓞ orcid.org/0000-0003-3456-3787

**Sara Santiago** − *Institut de Microelectrònica de Barcelona (IMB-CNM, CSIC), Universitat Autònoma de Barcelona,*

*08193 Cerdanyola del Vallès (Barcelona), Spain; Departament de Química, Universitat Autònoma de Barcelona, 08193 Cerdanyola del Vallès (Barcelona), Spain*

**Xavier Muñoz-Berbel** − *Institut de Microelectrònica de Barcelona (IMB-CNM, CSIC), Universitat Autònoma de Barcelona, 08193 Cerdanyola del Vallès (Barcelona), Spain;* ⓞ orcid.org/0000-0002-6447-5756

Complete contact information is available at:
https://pubs.acs.org/10.1021/acsomega.1c03434

### Notes

The authors declare no competing financial interest.

## ■ REFERENCES

(1) Ahmed, A.; Rushworth, J. V.; Hirst, N. A.; Millner, P. A. Biosensors for Whole-Cell Bacterial Detection. *Clin. Microbiol. Rev.* **2014**, *27*, 631−646.

(2) Roszak, D. B.; Colwell, R. R. Metabolic Activity of Bacterial Cells Enumerated by Direct Viable Count. *Appl. Environ. Microbiol.* **1987**, *53*, 2889−2893.

(3) Chiquet, C.; Cornut, P.; Benito, Y.; Thuret, G.; Maurin, M.; Lafontaine, P.; Pechinot, A.; Palombi, K.; Lina, G.; Bron, A.; Denis, P.; Carricajo, A.; Creuzot, C. Eubacterial PCR for Bacterial Detection and Identification in 100 Acute Postcataract Surgery Endophthalmitis. *Invest. Ophthalmol. Visual Sci.* **2008**, *49*, 1971−1978.

(4) Wyatt, G. M.; Langley, M. N.; Lee, H. A.; Morgan, M. R. A. Further Studies on the Feasibility of One-Day Salmonella Detection by Enzyme-Linked Immunosorbent Assay. *Appl. Environ. Microbiol.* **1993**, *59*, 1383−1390.

(5) Tong, R.; Zhang, L.; Song, Q.; Hu, C.; Chen, X.; Lou, K.; Gong, X.; Gao, Y.; Wen, W. A Fully Portable Microchip Real-Time Polymerase Chain Reaction for Rapid Detection of Pathogen. *Electrophoresis* **2019**, *40*, 1699−1707.

(6) Mao, X.; Yang, L.; Su, X. L.; Li, Y. A Nanoparticle Amplification Based Quartz Crystal Microbalance DNA Sensor for Detection of Escherichia Coli O157:H7. *Biosens. Bioelectron.* **2006**, *21*, 1178−1185.

(7) Shirasu, K. The HSP90-SGT1 Chaperone Complex for NLR Immune Sensors. *Annu. Rev. Plant Biol.* **2009**, *60*, 139−164.

(8) Soejima, T.; Iida, K. I.; Qin, T.; Taniai, H.; Seki, M.; Yoshida, S. I. Method to Detect Only Live Bacteria during PCR Amplification. *J. Clin. Microbiol.* **2008**, *46*, 2305−2313.

(9) Vang, Ó. K.; Corfitzen, C. B.; Smith, C.; Albrechtsen, H. J. Evaluation of ATP Measurements to Detect Microbial Ingress by Wastewater and Surface Water in Drinking Water. *Water Res.* **2014**, *64*, 309−320.

(10) Tambi, A.; Brighu, U.; Gupta, A. B. MColiPAT Kit for Early Detection of Coliforms in Water. *Water Sci. Technol.: Water Supply* **2020**, *20*, 871−877.

(11) Hua, X.-W.; Bao, Y.-W.; Wang, H.-Y.; Chen, Z.; Wu, F.-G. Bacteria-Derived Fluorescent Carbon Dots for Microbial Live/Dead Differentiation. *Nanoscale* **2017**, *9*, 2150−2161.

(12) Chen, X.; Zhang, X.; Li, C.; Sayed, S. M.; Sun, W.; Lin, F.; Wu, F.-G. Superbright Organosilica Nanodots as a Universal Sensor for Fast Discrimination and Accurate Quanti Fi Cation of Live / Dead Cells. *Sens. Actuators, B* **2019**, *295*, 49−55.

(13) Dietvorst, J.; Vilaplana, L.; Uria, N.; Marco, M. P.; Muñoz-Berbel, X. Current and Near-Future Technologies for Antibiotic

Susceptibility Testing and Resistant Bacteria Detection. *TrAC, Trends Anal. Chem.* **2020**, *127*, No. 115891.

(14) Pujol-Vila, F.; Dietvorst, J.; Gall-Mas, L.; Díaz-González, M.; Vigués, N.; Mas, J.; Muñoz-Berbel, X. Bioelectrochromic Hydrogel for Fast Antibiotic-Susceptibility Testing. *J. Colloid Interface Sci.* **2018**, *511*, 251−258.

(15) Pujol-Vila, F.; Giménez-Gómez, P.; Santamaria, N.; Antúnez, B.; Vigués, N.; Díaz-González, M.; Jiménez-Jorquera, C.; Mas, J.; Sacristán, J.; Muñoz-Berbel, X. Portable and Miniaturized Optofluidic Analysis System with Ambient Light Correction for Fast in Situ Determination of Environmental Pollution. *Sens. Actuators, B* **2016**, *222*, 55−62.

(16) Deiss, F.; Funes-Huacca, M. E.; Bal, J.; Tjhung, K. F.; Derda, R. Antimicrobial Susceptibility Assays in Paper-Based Portable Culture Devices. *Lab Chip* **2014**, *14*, 167−171.

(17) Pujol-Vila, F.; Vigués, N.; Guerrero-Navarro, A.; Jiménez, S.; Gómez, D.; Fernández, M.; Bori, J.; Vallès, B.; Riva, M. C.; Muñoz-Berbel, X.; Mas, J. Paper-Based Chromatic Toxicity Bioassay by Analysis of Bacterial Ferricyanide Reduction. *Anal. Chim. Acta* **2016**, *910*, 60−67.

(18) Patil, Sa.; Hägerhäll, C.; Gorton, L. Electron Transfer Mechanisms between Microorganisms and Electrodes in Bioelectrochemical Systems. *Bioanal. Rev.* **2012**, *4*, 159−192.

(19) Sydow, A.; Krieg, T.; Mayer, F.; Schrader, J.; Holtmann, D. Electroactive Bacteria — Molecular Mechanisms and Genetic Tools. *Appl. Micobiol. Biotechnol.* **2014**, *98*, 8481−8495.

(20) Rawson, F. J.; Downard, A. J.; Baronian, K. H. Electrochemical Detection of Intracellular and Cell Membrane Redox Systems in Saccharomyces Cerevisiae. *Sci. Rep.* **2014**, *4*, No. 5216.

(21) Morris, K.; Catterall, K.; Zhao, H.; Pasco, N.; John, R. Ferricyanide Mediated Biochemical Oxygen Demand - Development of a Rapid Biochemical Oxygen Demand Assay. *Anal. Chim. Acta* **2001**, *442*, 129−139.

(22) Morris, K.; Zhao, A. H.; A, R. J. Ferricyanide-Mediated Microbial Reactions for Environmental Monitoring. *Aust. J. Chem.* **2005**, *58*, 237−245.

(23) Yoshida, N.; Yano, K.; Morita, T.; Mcniven, S. J.; Nakamura, H.; Karube, I. A Mediator-Type Biosensor as a New Approach to Biochemical Oxygen Demand Estimation. *Analyst* **2000**, *125*, 2280−2284.

(24) Rosseinsky, D. R.; Glasser, L.; Jenkins, H. D. B. Thermodynamic Clarification of the Curious Ferric/Potassium Ion Exchange Accompanying the Electrochromic Redox Reactions of Prussian Blue, Iron(III) Hexacyanoferrate(II). *J. Am. Chem. Soc.* **2004**, *126*, 10472−10477.

(25) Ding, P.; Song, G.; Zhou, J.; Song, Q. Collection of Rolling Fingerprints by the Electrochromism of Prussian Blue. *Dye. Pigm.* **2015**, *120*, 169−174.

(26) Itaya, K.; Uchida, I.; Neff, V. D. Electrochemistry of Polynuclear Transition Metal Cyanides: Prussian Blue and Its Analogues. *Acc. Chem. Res.* **1986**, *19*, 162−168.

(27) Ricci, F.; Palleschi, G. Sensor and Biosensor Preparation, Optimisation and Applications of Prussian Blue Modified Electrodes. *Biosens. Bioelectron.* **2005**, *21*, 389−407.

(28) Karyakin, A. A. Advances of Prussian Blue and Its Analogues in (Bio)Sensors. *Curr. Opin. Electrochem.* **2017**, *5*, 92−98.

(29) Koncki, R. Chemical Sensors and Biosensors Based on Prussian Blues. *Crit. Rev. Anal. Chem.* **2002**, *32*, 79−96.

(30) Jahn, M. K.; Haderlein, S. B.; Meckenstock, R. U. Reduction of Prussian Blue by the Two Iron-Reducing Microorganisms Geobacter Metallireducens and Shewanella Alga. *Environ. Microbiol.* **2006**, *8*, 362−367.

(31) Ferrer-vilanova, A.; Alonso, Y.; Dietvorst, J.; Pérez-montero, M.; Rodríguez-rodríguez, R.; Ivanova, K.; Tzanov, T.; Vigués, N.; Mas, J.; Guirado, G.; Muñoz-berbel, X. Sonochemical Coating of Prussian Blue for the Production of Smart Bacterial- Sensing Hospital Textiles. *Ultrason. Sonochem.* **2021**, *70*, No. 105317.

(32) Ellis, D.; Eckhoff, M.; Neff, V. D. Electrochromism in the Mixed-Valence Hexacyanides. 1. Voltammetric and Spectral Studies of the Oxidation and Reduction of Thin Films of Prussian Blue. *J. Phys. Chem. A.* **1981**, *85*, 1225−1231.

(33) Karyakin, A. A. Prussian Blue and Its Analogues: Electrochemistry and Analytical Applications. *Electroanal.* **2001**, *13*, 813−819.

(34) Ware, M. Prussian Blue: Artists' Pigment and Chemists' Sponge. *J. Chem. Educ.* **2008**, *85*, No. 612.

(35) Kohn, M. New Observations on the Solubility of Prussian Blue. *Anal. Chim. Acta* **1954**, *11*, 18−27.

(36) Kracke, F.; Vassilev, I.; Krömer, J. O. Microbial Electron Transport and Energy Conservation - The Foundation for Optimizing Bioelectrochemical Systems. *Front. Microbiol.* **2015**, *6*, No. 575.

(37) Ramsay, G.; Turner, A. P. F. Development of an Electrochemical Method for the Rapid Determination of Microbial Concentration and Evidence for the Reaction Mechanism. *Anal. Chim. Acta* **1988**, *215*, 61−69.

(38) Dacarro, G.; Taglietti, A. Prussian Blue Nanoparticles as a Versatile Photothermal Tool. *Molecules* **2018**, *23*, No. 1414.

(39) Mortimer, R. J.; Rosseinsky, D. R. Iron Hexacyanoferrate Films: Spectroelectrochemical Distinction and Electrodeposition Sequence of "Soluble" (K+-Containing) and "Insoluble" (K+-Free) Prussian Blue, and Composition Changes in Polyelectrochromic Switching. *J. Chem. Soc. Dalt. Trans.* **1984**, 2059−2062.

(40) Bueno, P. R.; Ferreira, F. F.; Giménez-Romero, D.; Faria, R. C.; Gabrielli, C.; et al.et al. Synchrotron structural characterization of electrochemically synthesized hexacyanoferrates containing K+: A revisited analysis of electrochemical redox. *J. Phys. Chem. C* **2008**, *112* (34), 13264−13271.

(41) DeLongchamp, D. M.; Hammond, P. T. High-Contrast Electrochromism and Controllable Dissolution of Assembled Prussian Blue/Polymer Nanocomposites. *Adv. Funct. Mater.* **2004**, *14*, 224−232.

(42) García-Jareño, J. J.; Navarro-Laboulais, J.; Vicente, F. Electrochemical Study of Nafion Membranes/Prussian Blue Films on Ito Electrodes. *Electrochim. Acta* **1996**, *41*, 2675−2682.

(43) Zargar, B.; Hatamie, A. Prussian Blue Nanoparticles: A Simple and Fast Optical Sensor for Colorimetric Detection of Hydralazine in Pharmaceutical Samples. *Anal. Methods* **2014**, *6*, 5951−5956.

(44) Berney, M.; Hammes, F.; Bosshard, F.; Weilenmann, H. U.; Egli, T. Assessment and Interpretation of Bacterial Viability by Using the LIVE/DEAD BacLight Kit in Combination with Flow Cytometry. *Appl. Environ. Microbiol.* **2007**, *73*, 3283−3290.

(45) Liu, X.; Marrakchi, M.; Xu, D.; Dong, H.; Andreescu, S. Biosensors Based on Modularly Designed Synthetic Peptides for Recognition, Detection and Live/Dead Differentiation of Pathogenic Bacteria. *Biosens. Bioelectron.* **2016**, *80*, 9−16.

(46) Davidson, D.; Welo, L. A. The Nature of Prussian Blue. *J. Phys. Chem. B.* **1928**, *32*, 1191−1196.

(47) Pellitero, M. A.; Guimerà, A.; Kitsara, M.; Villa, R.; Rubio, C.; Lakard, B.; Doche, M. L.; Hihn, J. Y.; Del Campo, F. J. Quantitative Self-Powered Electrochromic Biosensors. *Chem. Sci.* **2017**, *8*, 1995−2002.

(48) Garcia-Jareno, J. J.; Benito, D.; Navarro-Laboulais, J.; Vicente, F. Electrochemical Behavior of Electrodeposited Prussian Blue Films on ITO Electrode: An Attractive Laboratory Experience. *J. Chem. Educ.* **1998**, *75*, 881.